Shaking Table Tests on “THE Structural Control System Using Double Core Column”

Yuta Kurokawa*1 Takayuki Sone*2 Yu Suzuki*3
Hiroki Hamaguchi*4 Masashi Yamamoto*5 Tatsuhiko Maeda*6

Summary

The system, “THE (Takenaka High-grade Earthquake resistant system) Structural Control System Using Double Core Column” for high rise buildings is under development. In this system, a damping layer is provided between a rigid upper core column suspended from the top of the building and a rigid lower core column stood up from the building foundation, whereby the responses equivalent to the top floor generate in the damping layer, and by installing dampers intensively to there, high damping effect is exhibited. In this report, shaking table tests using the scaled test specimens, which simulate a building, were conducted in order to verify the damping effect and to confirm the difference of the effect due to the damping coefficient of the damper. Furthermore, analysis was performed using an analysis model that can simulate the test results. In conclusion, it was verified that this system can reduce mainly the response of the first mode, and that the optimal damping coefficient for the maximum damping effect exists.

Keywords: structural control, damping effect, core column, shaking table test

1 Introduction

Long-period ground motion (e.g., Nankai trough earthquake and Sagami trough earthquake), whose potential occurrence has been of concern in recent years, has been suggested to have a potential magnitude that exceeds the ground motion levels specified in the Building Standards Law[1]. In these scenarios, high-rise buildings will be struck by seismic forces that exceed conventional predictions, requiring these buildings to improve seismic performance.

A structural control system has often been used to increase the seismic performance of high-rise buildings. The dampers installed in each story provide damping force that depends on inter-story drift and velocity in standard structural control building. However, there are architectural limits to the number of dampers that can be installed in each story, and the inter-story drift of each floor is small relative to displacement of the entire building. Consequently, the amount of additional damping is limited in the case of installing dampers in each story. We devised the “THE (Takenaka High-grade Earthquake resistant system) structural control system using double core column” (henceforth, “system”) that produces significant damping. An overview of the system is shown in Fig. 1. A damping layer is provided between a rigid upper core column suspended from the top of the building and a rigid lower core column standing up from the building foundation, whereby the responses equivalent to the top floor are generated in the damping layer, and greatly improved damping performance of the building due to the concentrated installation of dampers.

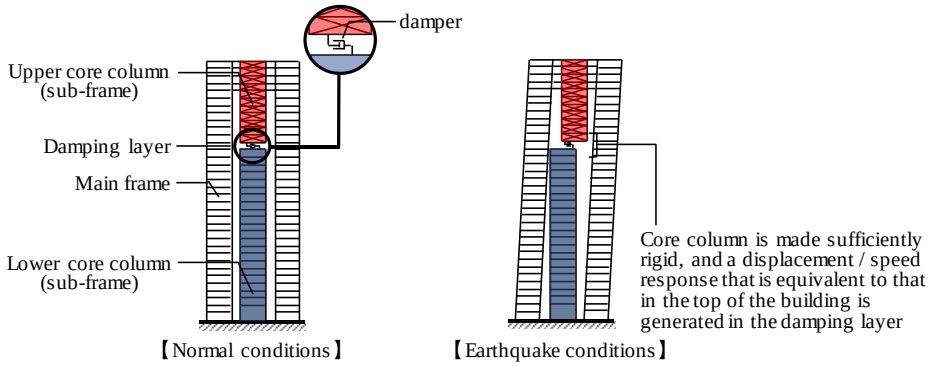

Fig.1 Outline of the system “THE *Structural Control System Using Double Core Column*”

＊1 Associate Chief Researcher, Research & Development Institute
＊2 Chief Researcher, Research & Development Institute
＊3 Researcher, Research & Development Institute, Dr. Eng.
＊4 Group Leader, Research & Development Institute, Dr. Eng.
＊5 General Manager, Earthquake Engineering Department, Research & Development Institute, Dr. Eng.
＊6 Assistant General Manager, Structural Design Department, Osaka Main Office

Previous analytical investigations have indicated the effectiveness of the system[2]. Among these, the damping coefficient of the damper in this system has been shown to have an optimal value for maximizing structural control performance. This study reports on results of shaking table tests conducted to verify the structural control effects due to the present system and to confirm the differences in damper coefficients. An analytical model was also created to simulate the experimental results, showing the variation of responses due to the different damping coefficients.

2 Experimental Overview

2.1 Outline of Test Specimen

An overall view of the specimen is shown in Photo 1, schematic diagrams of the specimen are shown in Fig. 2, and the specifications of the specimen are shown in Table 1. As shown in Fig. 2(d), we prepared eight boxes comprising two square-shaped steel plates with square hole linked with four H steel columns. As shown in Fig. 2(a), one of these boxes was fixed to the shaking table and set as the podium, while the other seven boxes were stacked on top of the podium as seven stories through a linear guide and coiled spring, simulating the structure shown in Fig. 1. The coiled spring rigidity was set so that the first natural period of the specimen without damper in the damping layer was approximately three seconds. A 350-mm square steel tube simulating the upper core column in Fig. 1 was suspended from the seventh story box, and its mass is larger than the other boxes. Similar to the upper core column, the lower core column was simulated with a 350-mm square steel tube and stood from the shaking table.

As shown in Fig. 2(b), the damping layer between the upper and lower core columns accommodates an oil damper. The present experiment was conducted under three conditions: no damper installed, a velocity-dependent damper with a damping coefficient C_L = 2.23 kN･s/m, and a velocity-dependent damper with a damping coefficient C_H = 6.37 kN･s/m. The damping coefficient C_L was approximately equivalent to the optimal value for minimizing inter-story drifts calculated from analyses using the properties shown in Table 1.

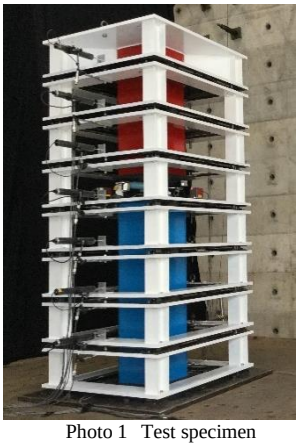

Photo 1 Test specimen

Table 1 Specifications of test specimen

Story number	Mass (kg)	Stiffness (kN/m)
7	600	16.6
6	200	
5		27.2
4		
3		40.8
2		
1		

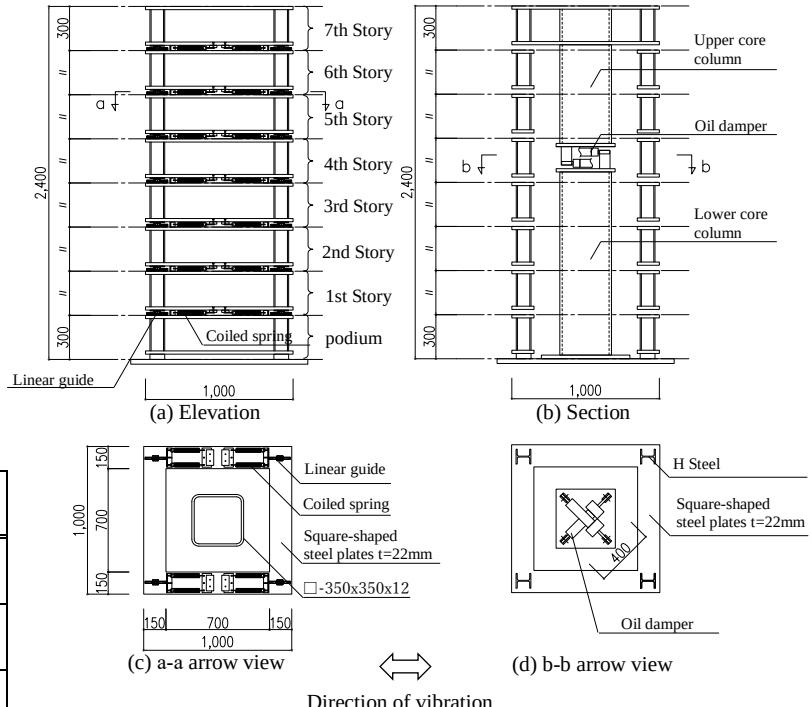

Fig.2 Schematic diagrams of test specimen

2.2 Outline of Excitation Wave for Experiment

Uniaxial excitations in the direction shown in Fig. 2 were conducted using a 1,000 kN actuator attached to a shaking table. The four excitation waves described in Table 2 were selected in order to confirm whether the damping effect of system was affected by the difference in seismic motion characteristics. The input level of each excitation wave was adjusted so that the maximum inter-story drift of the specimen was approximately 30 mm without dampers in the damping layer. The velocity waveforms of the excitation waves are shown in Fig. 3, and the system acceleration response spectrum (excluding the sweep waves) is shown in Fig. 4.

Table 2 Outline of input waves

Excitation wave	Summary
Sweep wave	Gradually increasing sin wave of 0.1 Hz – 5 Hz used for determining the characteristics of the specimen
Kokuji wave - random	Simulated ground motion on engineering bedrock is generated according to notifications[3)], and input ground motion was created at a building foundation level using a surface layer ground model corresponding to the OS1 region within Osaka city
OS1	Long-period ground motion OS1 wave indicated in the technical advice[1)] of the Japanese Ministry of Land, Infrastructure and Transport was used in the surface layer ground model in the OS1 region within Osaka city as a wave in the building foundation level, of which the essential 300-s period was extracted and used as an input wave
Uemachi 3B pulse-type	Uemachi 3B pulse-type input ground motion assuming ground motion of an inland earthquake, according to the Osaka Earthquake Study Group[4)]

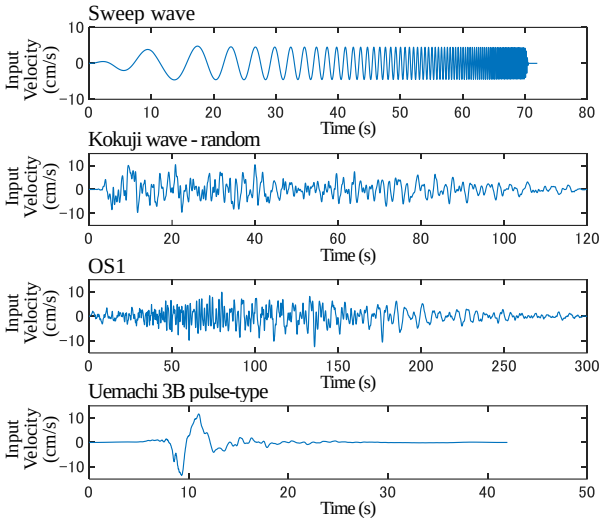

Fig.3 Input waveforms

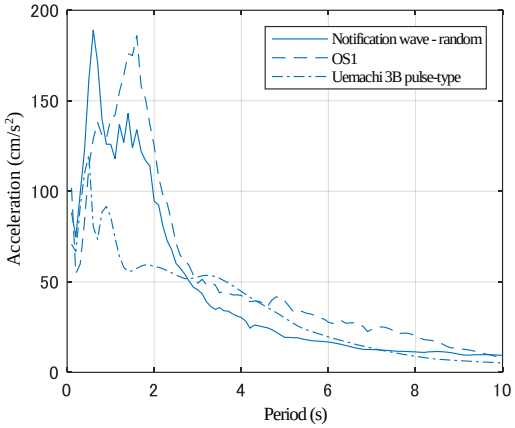

Fig.4 Acceleration response spectrum of input waves (h=0.05)

2.3 Measurement Overview and Experimental Case

The accelerations on each box and the shaking table in the excitation direction were measured with accelerometers, and the relative displacements between adjacent boxes were measured with displacement transducers. The sampling rate of the measurements was 100 Hz.

The following conditions of the specimen were implemented for the above-mentioned four excitation wave types: without damper, with damper of the damping coefficient C_L, and with damper of the damping coefficient C_H.

3 Experimental Results

3.1 Confirmation of Specimen Characteristics

The experimental results from the sweep wave excitations were used to confirm the specimen characteristics when no damper was used. The relationships between the story shear force and the inter-story drift of the 1st, 4th, and 7th stories are shown as representative examples in Fig. 5. The story shear force of each story was determined by calculating the box inertial force by multiplying the acceleration of each box with its mass, and summing all box inertial force above each story. The hysteretic behavior of each story exhibited a parallelogram-like shape, and its value was thought to be the sum of the linear spring characteristics of the coiled spring and the frictional characteristics of the linear guide.

Spring stiffness was identified by using the least-squares method from the story shear force-inter-story drift relationships of each story. The inter-story drift was multiplied by the identified spring stiffness to determine the restoring force due to the coiled spring, and the frictional force of the linear guide was determined as the story shear force minus the restoring force of the coiled spring. Frictional force-inter-story drift relationships where the frictional force of the linear guide is set as the vertical axis are shown in Fig. 6. The dotted lines in the figure indicate the identified frictional force of the linear guide. The identified frictional force was set to a value where the hysteretic area of the frictional force-inter-story drift is equal to the hysteretic area of the linear guide when the frictional characteristics show completely elasto-plastic.

The spring stiffness and frictional coefficient of each story are shown in Table 3. The frictional coefficient was determined by dividing the frictional force by the weight supported by each story. There was minimal variation between the measured and the designed values, indicating that the system performed as expected.

The transfer functions of each story for the acceleration of the shaking table are shown in Fig. 7. The first natural period was T_1=3.00 s (0.333 Hz), and the second natural period T_2=1.06 s (0.947 Hz). The second mode amplitude was largest in the 4th story placed at the antinode. The response of the third mode onwards was small, and no clear peaks were confirmed.

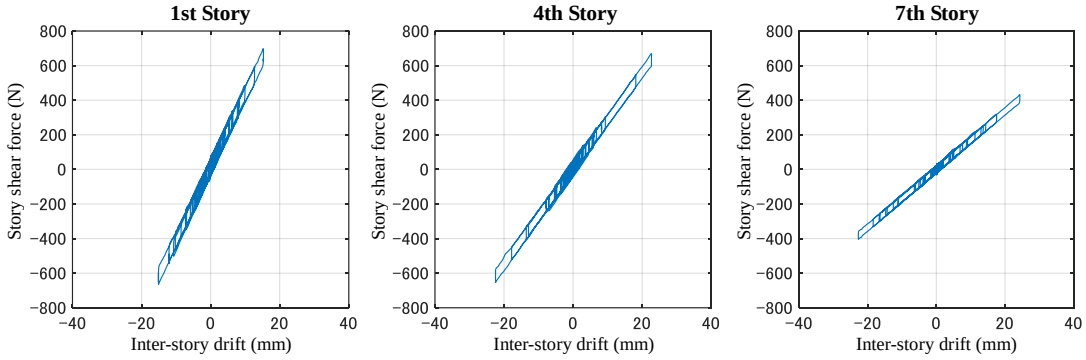

Fig.5 Shear force-inter-story drift relationships without damper

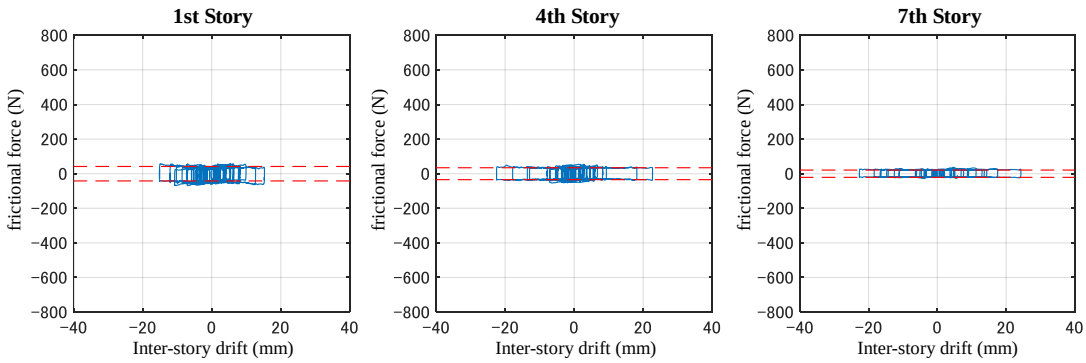

Fig.6 Shear force-inter-story drift relationships of linear guide elements in each story

Table 3 Identified results of stiffness in coil springs and coefficient of friction in linear guides in each story

Story number	Stiffness		Frictional Coefficient	
	Design value (kN/m)	Identified value (kN/m)	Design value (-)	Identified value (-)
7	16.6	16.86	3/1000	3.57/1,000
6		16.89		3.30/1,000
5	27.2	27.73		2.82/1,000
4		27.76		2.93/1,000
3	40.8	41.98		2.91/1,000
2		42.18		2.65/1,000
1		42.33		2.37/1,000

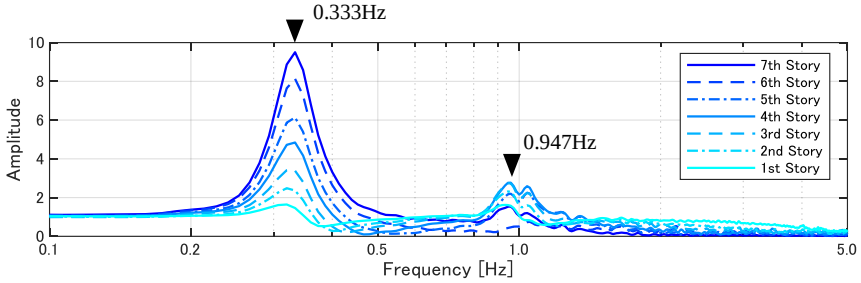

Fig.7 Transfer function at each story in specimen without damper

3.2 Damping Effect Analysis

The damping effect was analyzed by comparing the response results with and without the damper and the difference in the damping coefficient of the damper.

3.2.1 Maximum Response

The maximum responses obtained from each vibrational result are shown in Fig. 8 – Fig. 10. Results with damping coefficient of C_L or C_H, and without the damper are shown together. Fig. 8 and Fig. 9 show that response displacement greatly decreases independent of the excitation wave by installing a damper in the damping layer. Fig. 8 shows that for C_L the inter-story drift for each story is small independent of the excitation wave, whereas for C_H the inter-story drift near the 4th story placed at the antinode of the second mode is small, while the inter-story drift increases as it approached to the top and the 1st story. The maximum inter-story drift including all stories was smaller with damping coefficient C_L as compared to C_H. Fig. 9 shows that for C_H, the maximum relative displacement of the top was smaller than the middle layers such as the 4th story, independent of excitation wave. Fig. 10 shows that there were no major differences in maximum acceleration, independent of damper presence or excitation wave.

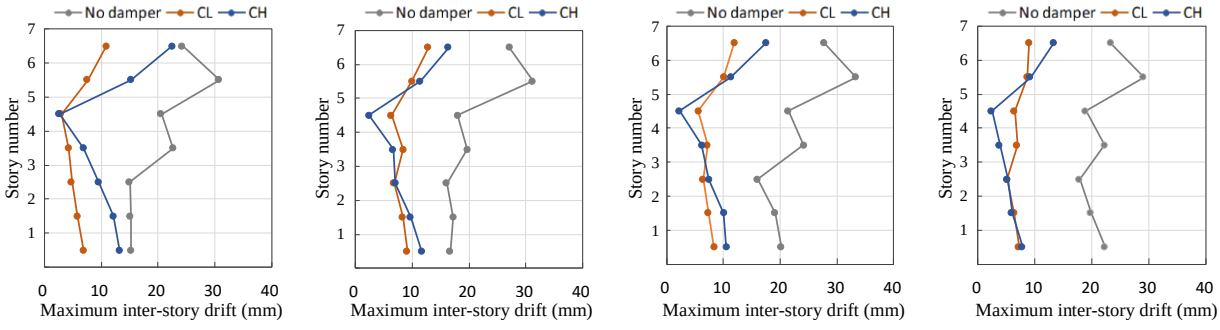

(a) Sweep wave (b) Kokuji wave - random (c) OS1 (d) Uemachi 3B pulse-type

Fig.8 Maximum inter-story drift

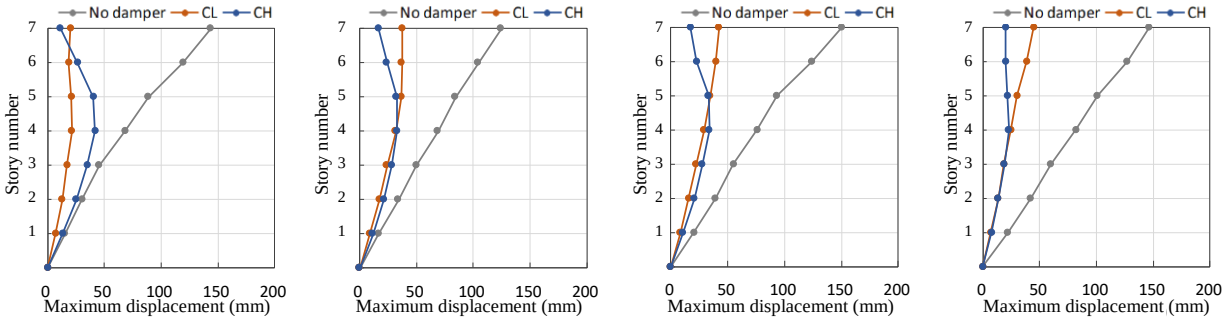

(a) Sweep wave (b) Kokuji wave - random (c) OS1 (d) Uemachi 3B pulse-type

Fig.9 Maximum relative displacement

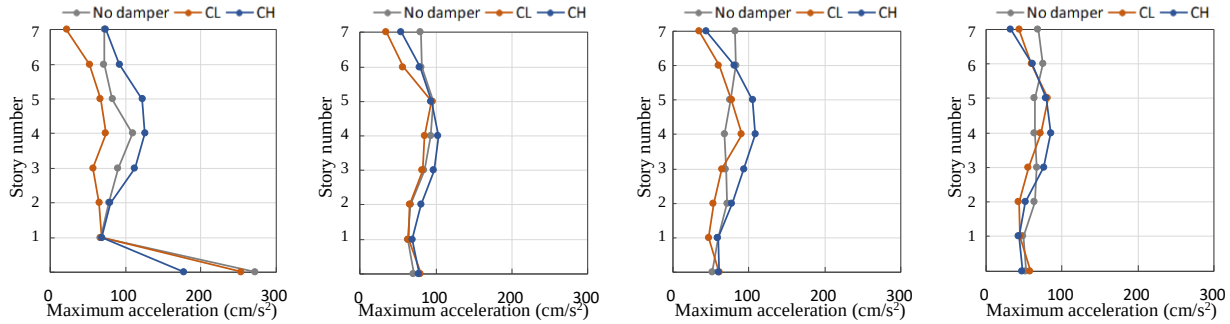

(a) Sweep wave (b) Kokuji wave - random (c) OS1 (d) Uemachi 3B pulse-type

Fig.10 Maximum absolute acceleration

3.2.2 Time History Inter-story Displacement Response

Time histories of the inter-story drift of the 4th and 7th story obtained from the sweep wave excitation results are shown in Fig. 11. Results with damping coefficient C_L or C_H, and when the damper was absent are shown together. Looking at the interval up to 40 s when the first mode response was prominent, the absence of dampers induced a prominent response as opposed to when the dampers were present (independent of the damping coefficient), indicating that the damper was effective for the first mode. Meanwhile, looking at the interval between 40 s and 50 s when the second mode response was prominent, the C_H response was greater than the damper-absent response. The C_L response was similar to the damper-absent response. This indicated that the damping effects were less for the second mode.

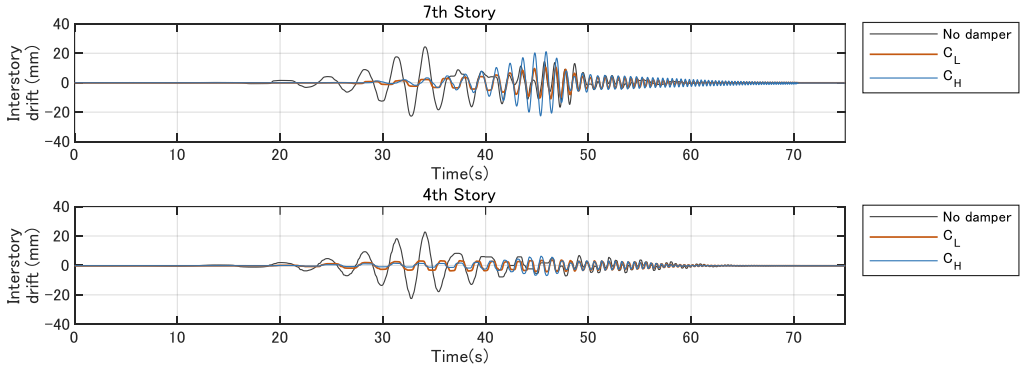

Fig.11 Time history waveforms of inter-story drift (during sweep wave)

3.2.3 Transfer Function

The transfer functions for the acceleration of the shaking table obtained from the sweep wave excitation results are shown in Fig. 12. Results with damping coefficients C_L or C_H, and when the damper was absent are shown together in the figure. The prominent amplitude at approximately 0.33 Hz was significantly reduced by installing a damper in the damping layer. Damping was extremely successful in the first mode. Results for the second mode at approximately 0.9 Hz in the 4th story show that C_L had an amplitude similar to that without the damper, but C_H had an amplitude that was larger than that without the damper. Here as well, the response results became smaller when the damper had a damping coefficient of C_L as opposed to C_H. There were no oscillations observed in the third or subsequent modes.

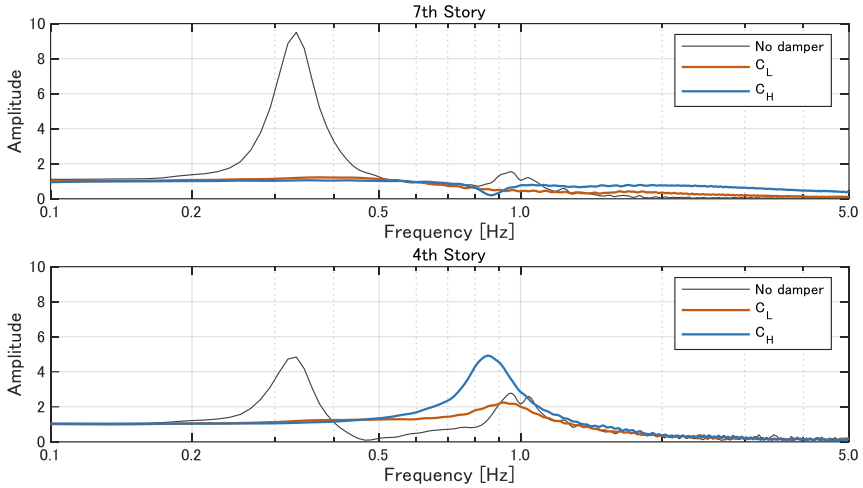

Fig.12 Comparison of transfer function with and without damper

4 Analytical Study

4.1 Analysis Model

Results for the two damping coefficients of C_L and C_H were obtained during experiments; moreover, parametric analysis was conducted to confirm the influence of the damping coefficient here. The analysis model was set as shown in Fig. 13,assuming that the sub-frames (upper core column and lower core column) are sufficiently rigid. A time history response analysis used the identified result values of stiffness and frictional coefficient shown in Table 3. The hysteretic characteristics of each story were set as bilinear model to account for the friction of the linear guide. The acceleration of the shaking table measured during the shaking table test was used for the input wave in the analysis.

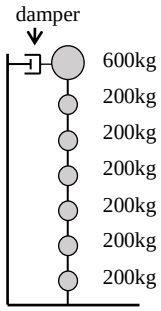

Fig.13 Analysis model

4.2 Comparisons with Experimental Results

The maximum responses of each input wave are shown in Fig. 14 – Fig. 16. The analysis results with the damper corresponded well with the experimental results for both damping coefficients C_L and C_H, and it was shown that the experimental results can be simulated using these analyses. The analysis results with the damper absent roughly corresponded with the experimental results, but inter-story drifts of each story were relatively large compared to the experimental results. This was thought to be because the damping characteristics of the specimen without a damper are influenced by the friction of the linear guide, whereas the frictional force of the linear guide in the analysis, which is assumed constant, actually has velocity-dependencies, and cannot be assumed as constant.

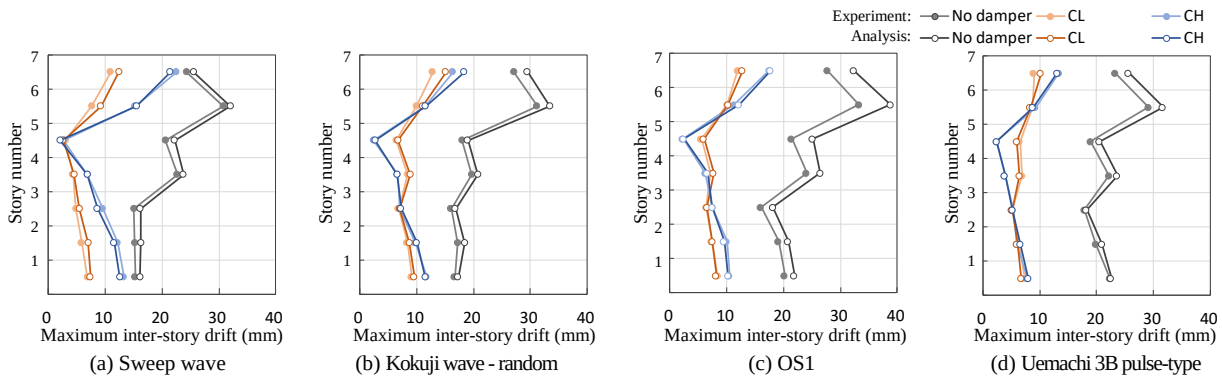

Fig.14 Maximum inter-story drift: analysis vs. experiment

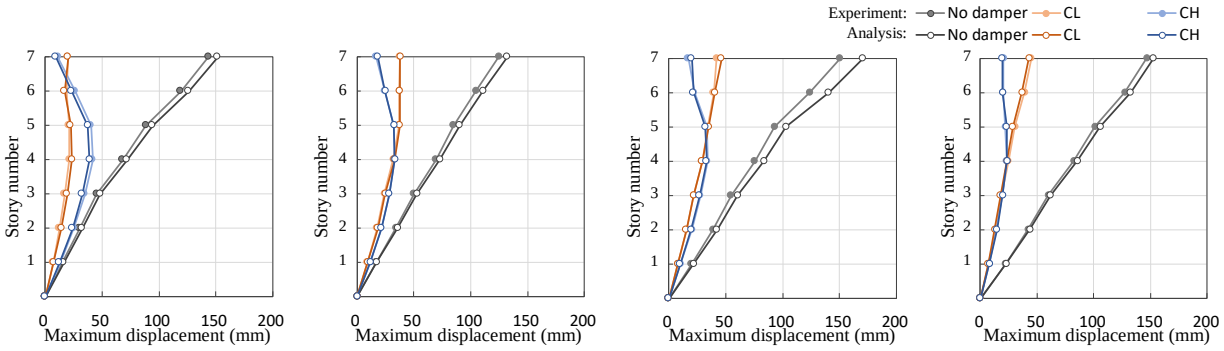

(a) Sweep wave (b) Kokuji wave - random (c) OS1 (d) Uemachi 3B pulse-type

Fig.15 Maximum relative displacement: analysis vs. experiment

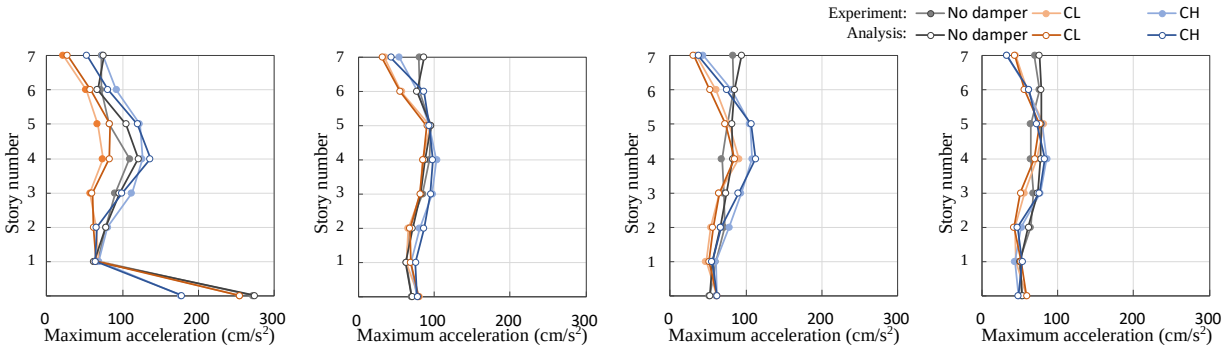

(a) Sweep wave (b) Kokuji wave - random (c) OS1 (d) Uemachi 3B pulse-type

Fig.16 Maximum absolute acceleration: analysis vs. experiment

4.3 Influence of Damping Coefficient

A parametric study was conducted where the damping coefficient of the damper was gradually increased from 0 to 20 kN / (m/s) in increments of 0.2. The relationships between the damping coefficients and the maximum response are shown in Fig. 17. Two dotted lines in the figure represent the position of the damping coefficient C_L and C_H. It can be seen that the damping coefficient C_L, which was set to minimize the maximum inter-story drift, was actually close to the optimal value. Furthermore, it can be seen that the optimal damping coefficient value of the damper for where the maximum inter-story drift is minimized and where the maximum relative displacement is minimized were different.

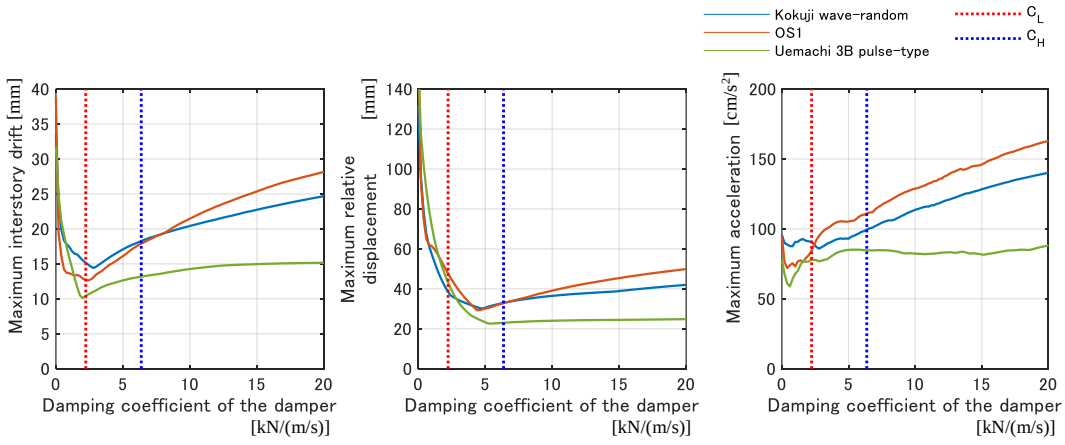

(a) Maximum inter-story drift (b) Maximum relative displacement (c) Maximum acceleration

Fig.17 Relationships between damping coefficient of damper and maximum responses

5 Conclusions

Shaking table tests were conducted on a system in which the acceleration and velocity responses equivalent to the top floor are generated during an earthquake in the damping layer, where a damper is intensively installed, through a firm sub-frames, to investigate the effectiveness of the system and to confirm the differences in the damping coefficient effectiveness of the damper. The results are summarized as follows.

(1) The system was particularly effective in controlling the first mode response and greatly decreased the inter-story drift of each layer.

(2) The system is effective for not only long-period ground motion, but also for ground motion determined by the Building Standards Law and ground motion of an inland earthquake.

(3) An optimum damping coefficient of a damper that maximizes the effectiveness of the system was confirmed.

References

1) Japanese Ministry of Land, Infrastructure and Transport Housing Bureau Building Guidance Section Chief: “High-rise building strategies against long-period ground motion generated by mega-earthquakes along the Nankai trough (technical advice)”, June 2016 (in Japanese)

2) Sone, T. et al. : “Damping systems of high-rise RC structures with increased damping efficiency of dampers using the displacement and velocity of the top of the building: Part (1)-(4)”, Summaries of technical papers of annual meeting of the Architectural Institute of Japan, Structure II, pp. 295-302, 2018.9 (in Japanese)

3) Japanese Ministry of Construction Notification No. 1461: “Designation of structure calculation standards for confirming the structural safety of high-rise buildings”, May 2000 (in Japanese)

4) Study group on earthquake motion and design method for building design against the inland earthquake in Osaka prefecture (Osaka Earthquake Study Group): “Earthquake ground motion and earthquake resistance design guidelines for building design against the inland earthquake in Osaka prefecture”. February 2015 (in Japanese)

Acknowledgments

Part of the present research was in collaboration with Takenaka Corporation and Kyoto University.

Appendix A

Fig. A1 shows the participation vectors and the natural periods without the damper and where the friction of the linear guide was ignored, determined by setting the analysis model as shown in Fig. 13 and conducting analyses using the properties of the specimen shown in Table 1. Furthermore, the results of the complex natural values obtained by including the damper (damping coefficient: C_L) and ignoring the friction of the linear guide are shown in Table A1. The damping ratio in the first mode is extremely large at 63%.

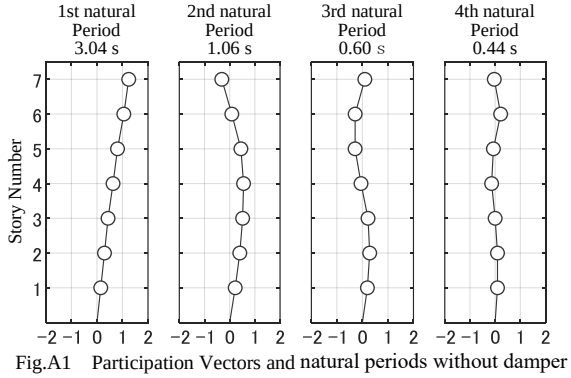

Fig.A1 Participation Vectors and natural periods without damper

Table A1 Natural periods and damping ratios with damper (Damping coefficient:C_L)

Order	Natural frequency (Hz)	Natural period (s)	Damping ratio
1	0.341	2.93	0.634
2	0.915	1.09	0.081
3	1.66	0.60	0.042
4	2.28	0.44	0.043